Microsystem Technologies 1 (1994) 2–9

Encapsulated micro mechanical sensors

Masayoshi Esashi

Abstract Encapsulated micro mechanical sensors were fabricated using glass-silicon anodic bonding and an electrical feedthrough structure. Two parallel plates which can be used not only for capacitive sensors but also electrostatic actuators are adopted for integrated sensors as capacitive pressure sensors, accelerometers and resonating sensors. Micromachining technologies were developed for these packaged micro sensors. These include silicon etching technologies as laser assisted etching, deep RIE and in-process thickness monitoring during wet etching. Anodic bonding technologies which enable to incorporate a circuit inside the package and to keep a sealed cavity at a high vacuum are also developed.

1
Introduction

Packaging is important for sensors not only to keep high stability but also to reduce the size and the fabrication cost [1. Esashi (1990)]. Glass-to-silicon anodic bonding is an important means of encapsulated sensors. It allows the silicon chip itself to be used as a package [2. Esashi et al. (1990)]. Not only small size but also low cost encapsulation by the batch process packaging at the wafer level can be achieved.

A capacitor is made of two parallel plate electrodes. One of them is the silicon diaphragm and the other being deposited on the glass. Such a parallel plates structure can be applied not only for capacitive sensors but also for electrostatically driven actuators. The insulating glass is suitable to reduce a stray capacitance and to increase a breakdown voltage. Applications of the parallel plates structure are capacitive pressure sensors, accelerometers including electrostatic servo control type and electrostatic self-diagnosis type, resonating sensors, Fabry–Perot interferometers and many other devices. In the following, some packaged sensors developed will be described. To detect small capacitances of micro capacitive sensors, capacitance detection circuits should be integrated. Fabrication processes which makes the integrated circuit compatible with the anodic bonding process and with the highly doped p^+ etch-stop process have to be developed.

Received: June 14, 1994/Accepted: July 8, 1994

M. Esashi
Faculty of Engineering, Tohoku University,
Aza-Aoba Aramaki Aoba-ku Sendai, 980 Japan

This work has been supported by the Japanese Ministry of Education Science and Culture under a Grand-in Aid No. 03102001

There are some special requirements for such structures: electrical feedthrough from the encapsulated cavity, distortion free bonding, vacuum pressure sealing, resistless dry etching to remove silicon partly after anodic bonding and so on. These micromachining technologies specially developed for the packaged micromechanical sensors will be also described.

2
Packaged Sensor

2.1
Pressure sensors

2.1.1
Integrated capacitive pressure sensor

[3 Matsumoto et al. (1990)]

Figure 1a shows the structure of an integrated capacitive pressure sensor. The silicon chip plays a role of not only a capacitive sensor and a substrate for a circuit but also a package. The spacing of the capacitor is as narrow as 2 μm to get high capacitance. Electrical feedthrough structure was needed to achieve hermeticity. CMOS capacitance detection circuit is integrated inside the hermetically shielded cavity, which performs high sensitivity and stability. Large capacitance change is available comparing with the resistance change of conventional piezoresistive sensors. The oscillation frequency of the circuit varies linearly with the pressure as shown in Fig. 1b.

Figure 2 shows the fabrication process. CMOS circuit is formed on a silicon wafer and the backside is patterned to form a diaphragm. After holes are formed through a glass plate by electrochemical discharge drilling, a Pt/Ti layer is formed for the capacitor electrode and for a plate to shield the circuit from illumination. If Al is used for the metal layer, hill-rocks are formed after the thermal treatment of the anodic bonding, causing the interference of the diaphragm motion. After the silicon wafer and the glass are bonded anodically, a diaphragm is formed by etching silicon. After separating each chip by dicing, two lead wires are installed at the glass holes. Using this method, the device fabrication is completed in the wafer stage (wafer process packaging) and a low-cost, small-sized device can be provided.

2.1.2
Capacitive vacuum sensors

[4. Henmi et al. (1993)]

On the contrary to piezoresistive pressure sensors of which diaphragm have to have piezoresistor, very thin diaphragm

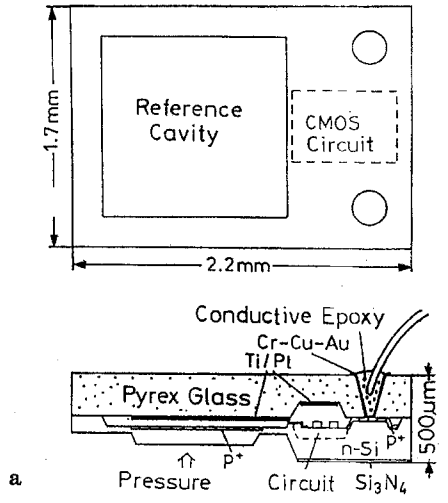

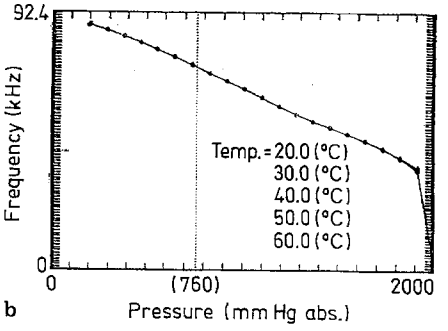

Fig. 1a, b. Integrated capacitive pressure sensor. a Structure; b Characteristic

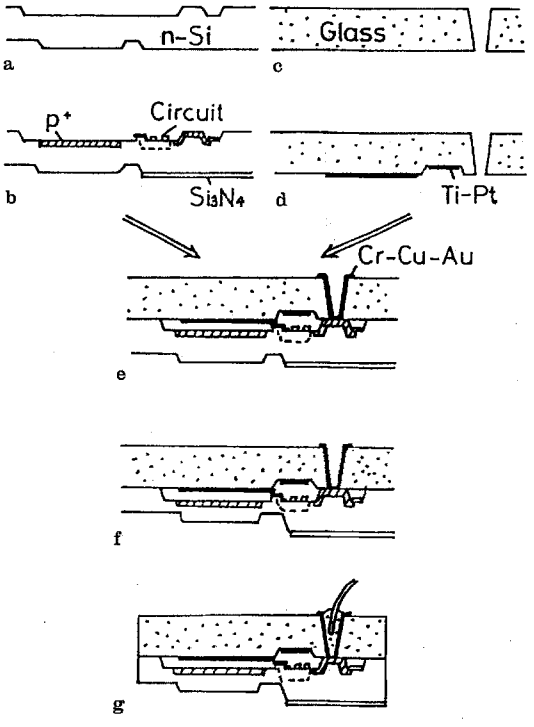

Fig. 2a–g. Fabrication process of integrated capacitive pressure sensor

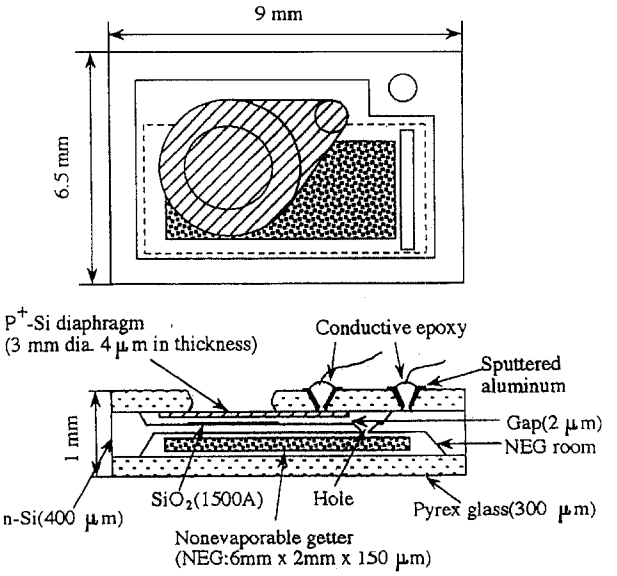

Fig. 3. Structure of capacitive vacuum sensor

formed by using p^+ etch-stop can be applied for capacitive pressure sensors. Therefore extremely high sensitive pressure sensors which can detect vacuum pressure can be realized. The structure of the capacitive vacuum sensor is shown in Fig. 3. Since vacuum sealed cavity is required, the sensor has a nonevaporable getter(NEG) in the cavity. The method to fabricate a vacuum sealed cavity will be described later.

2.2
Acceleration Sensors

[5. Esashi (1994)]

2.2.1
Integrated accelerometer with electrostatic servo

[6. Matsumoto et al. (1993)]

Figure 4 shows the structure of an integrated silicon capacitive accelerometer. This packaged accelerometer chip has a capacitive sensor for the displacement of the seismic mass, an integrated capacitance detection circuit, and an electrostatic actuator for force balancing or self-diagnosis. A silicon seismic mass is suspended with silicon-oxinitride(SiON) beams in fully symmetry. Small stoppers are formed on the surface to prevent the mass from sticking to the counter electrodes.

The capacitance detection circuit which has frequency output is designed not to be influenced by temperature and supply voltage, and to be used as two wires system of which current pulses in the power supply provides information about the frequency [7. Shirai et al. (1992)]. Similar circuit is also used for the integrated capacitive pressure sensor shown in Fig. 1.

The electrostatic servo system has been realized using the chip and an outer phase-locked-loop(PLL) servo circuit. The servo accelerometer enables to change the sensitivity by the feedback parameter and hence it provides wide dynamic range.

Internal stress of the SiON beam was controlled to have small stress in order to avoid buckling. The stress depends on the compositional ratio of oxide and nitride.

The different fabrication step of the accelerometer from that of pressure sensor shown in Fig. 2 is as follows. Deep silicon

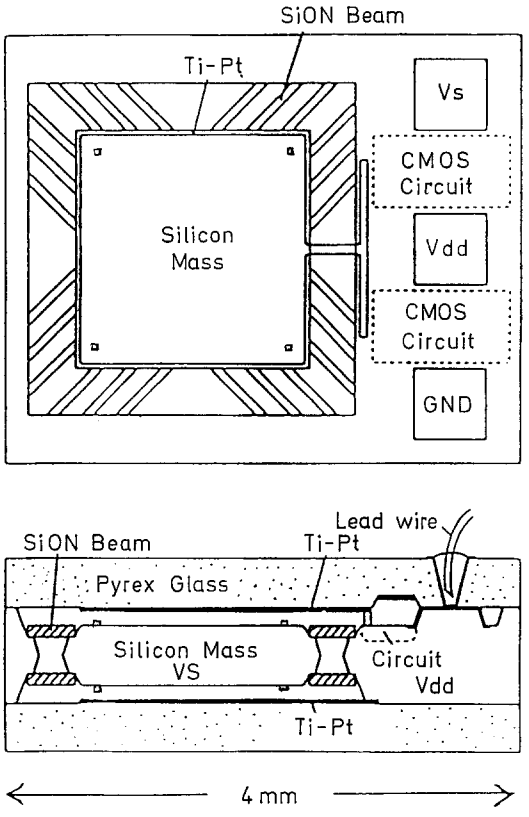

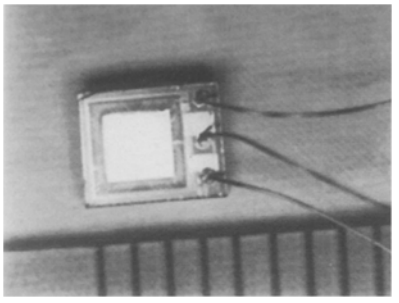

Fig. 4. Integrated capacitive accelerometer

etching have to be made before bonding a silicon to a glass. Therefore the circuit had to be protected from the etchant with spin-on-glass(SOG) during the etching period.

2.2.2
Three-axis electrostatic servo accelerometer

[8. Jono et al. (1994)]

A three-axis electrostatic force-balancing accelerometer was also developed with this packaging technology. The structure and the principle is shown in Fig. 5. The surrounding seismic mass is suspended from only center pillar with four thin silicon beams. Tilt of the mass by X or Y axis acceleration and movement by Z axis acceleration are detected capacitively. Differential capacitances are detected separately using phase sensitive detector. The feedback voltage for force balancing are superimposed on the signal voltages for capacitive sensing.

The dynamic response of the accelerometer depends on the internal pressure because of the squeezed film effect.

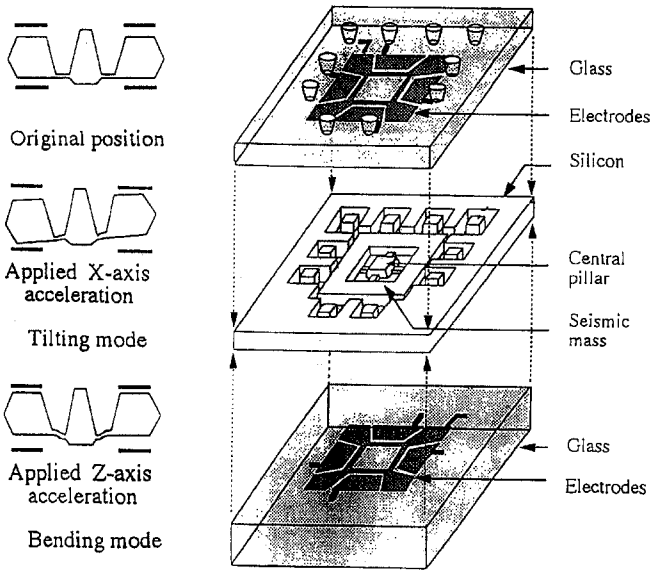

Fig. 5. Three-axis electrostatic servo accelerometer

Optimum pressure which avoids its resonance but have wide frequency response is required to be kept inside the cavity. The critical dumping condition of this sensor measured was about 1 torr [9. Mineta et al. (1993)].

2.3
Resonant sensors

2.3.1
Packaged resonator

[10. Yoshimi et al. (1992)]

Packaged micro resonator was fabricated using the feedthrough structure. The principle and the structure are shown in Fig. 6a and b respectively. A processed silicon wafer, containing a tortional resonator and the islands used for the electrical connection of the electrodes on the glasses, is sandwiched between two glass plates. The resonator is driven electrostatically and the movement is detected capacitively.

The pressure dependency of the quality (Q) factor of the resonator is shown in Fig. 6c. This indicates that the behavior of such a micro resonator is considerably influenced by the surrounding air and high vacuum sealing is required. The high vacuum sealing will be described below. The resonant sensor can be used as a vacuum sensor, however it is much influenced by the gas adsorption on the surface of the seismic mass. Silicon micro resonators can have very high quality factor because of their small internal friction. High quality factor leads to high resolution of resonant sensors.

2.3.2
Resonant infrared sensor

[11. Cabuz et al. (1993)]

When an optical power is incident on a microresonant structure, a photothermal induced stress which results in resonant frequency change is generated in the resonator. Infrared sensor or radiation temperature sensor using the principle was developed. The structure is shown in Fig. 7a. The resonator

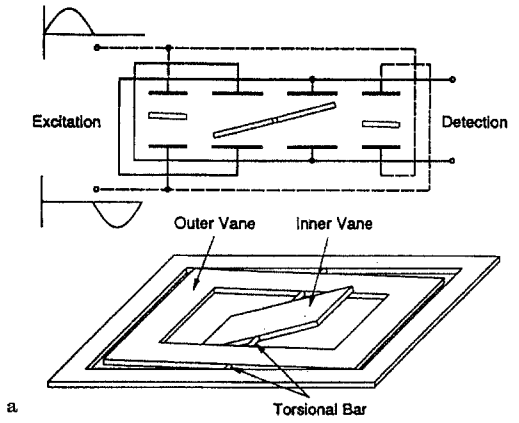

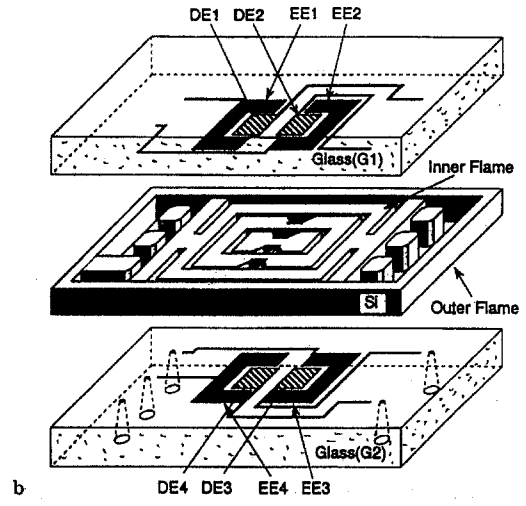

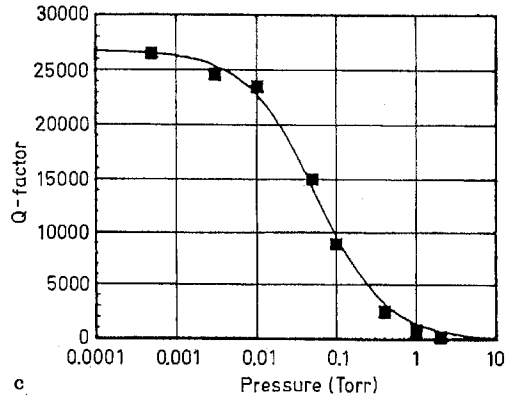

Fig. 6a–c. Packaged micro resonator. a Principle; b Structure; c Pressure dependence of the Q factor

bridge is clamped on a silicon frame of which one-side is bonded to the glass in order to avoid package stresses.

Good thermal isolation is required for high sensitivity. The resonator bridge consists of a p^+ silicon absorber supported with silicon dioxide beams from silicon frame. The SiO_2 beams isolate p^+ Si from the silicon frame not only electrically but also thermally. In order to realize high Q factor and good thermal isolation, the resonator is placed in vacuum. For this reason vacuum packaging described later is indispensable.

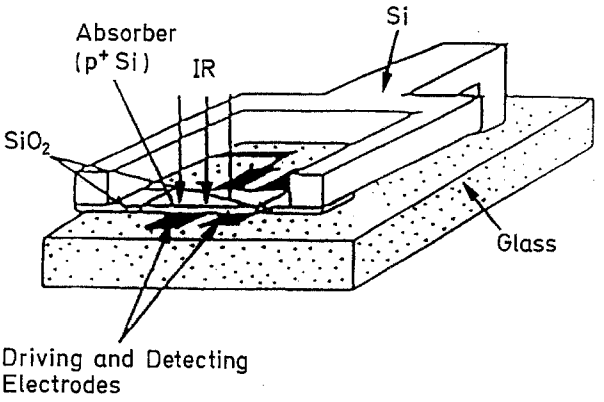

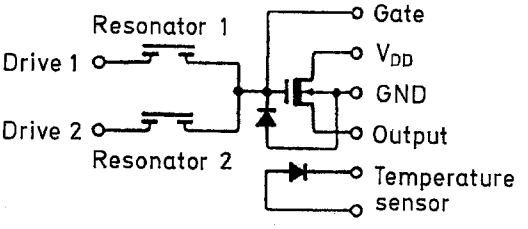

Fig. 7a, b. Resonant infrared sensor. a Resonator; b On-chip circuit

One port excitation/detection with a floating electrode on the resonator was used. A reference resonator for temperature compensation and on-chip detection transistor were integrated as shown in Fig. 7b. The resonant frequency and Q factor were about 100 kHz and 20,000. The responsivity was about 500 ppm/μW. Packaged micro resonators were fabricated using the feedthrough structure.

To realize highly sensitive resonant sensors the control of the intrinsic stress in the p^+ silicon film is essential. Microfocus Raman spectroscopy and other techniques were applied to study such mechanical properties [12. Cabuz et al. (1994)].

2.3.3
Silicon resonant angular rate sensor

[13. Hashimoto et al. (1994)]
Silicon resonant angular rate sensor was developed. The principle and the structure is shown in Fig. 8. The sensor is a tuning fork, both sides suspended with torsion bars. Electromagnetic excitation and capacitive detection are used. The applied angular rate generates the Coriolis' force and the resonator starts torsional vibration around the torsion bar.

3
Micromachining

3.1
Electrical feedthrough

The electrical feedthrough from the cavity was made through a glass hole as shown in Fig. 9a, b, c [14. Esashi et al. (1992)]. This vertical feedthrough structure can seal the cavity hermetically around the glass hole [2. Esashi et al. (1990)]. The glass holes can be made by electrochemical discharge drilling [15. Shoji et al. (1990)]. The feedthrough from the silicon

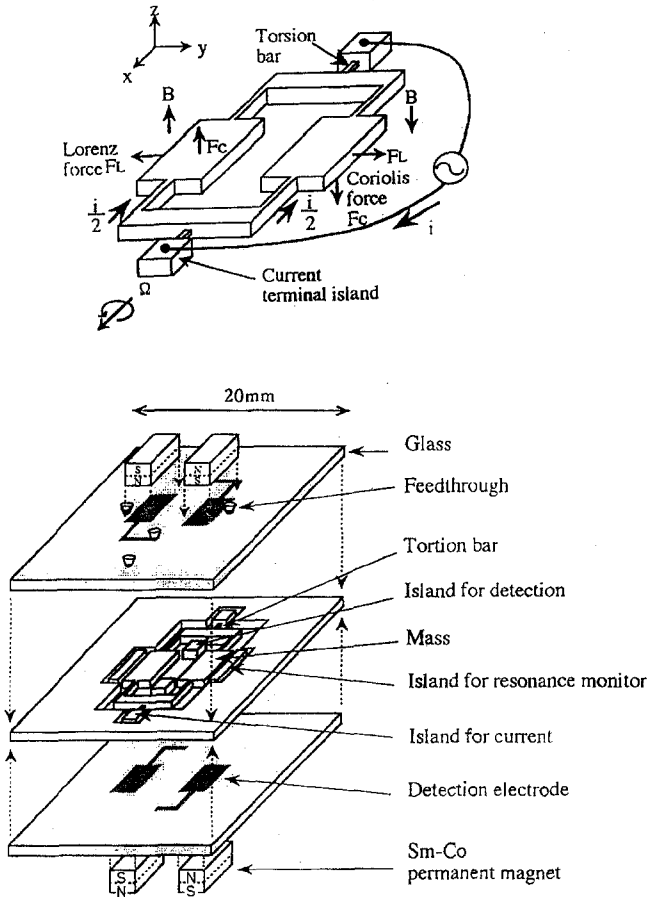

Fig. 8. Resonant Angular Rate Sensor

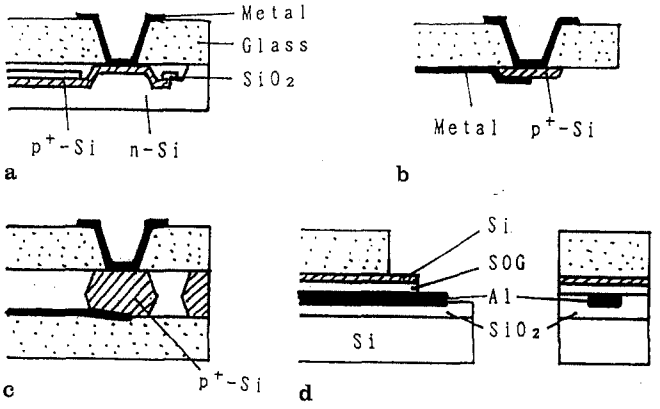

Fig. 9a–d. Electrical feedthrough from the packaged cavity. a Vertical feedthrough from silicon; b Vertical feedthrough from top glass electrode; c Vertical feedthrough from top or bottom glass electrode; d Lateral feedthrough

was made using diffusion layer of which pn junction is covered with SiO_2 as Fig. 9a. The feedthrough structures from the glass electrode are shown in Fig. 9b and c.

Another type lateral feedthrough shown in Fig. 9d was developed [14. Esashi et al. (1992)]. Al is embedded in a SiO_2 layer and then it is covered with a spin-on-glass(SOG) to insulate and to planerize the surface. After this step, the surface is covered with silicon by sputter deposition. Finally a glass is anodically bonded to the silicon layer. This lateral feedthrough realizes finer pitch pads and smaller series resistance than the vertical one.

3.2
Anodic bonding

3.2.1
Selective bonding

Since the seismic mass of accelerometer should not be bonded to the glass, we have to avoid a electrostatic force on the seismic mass. For this purpose, shield electrode on the glass is needed and it is connected to the silicon during anodic bonding process. It was possible to cut the connection through the glass by using YAG laser after packaging. Al, Pt/Cr and Pt/Ti could be used for the electrode because it stands the anodic bonding process.

3.2.2
Circuit compatible bonding

[16. Shirai et al. (1992)]

Electronic circuit has to stand the condition of the anodic bonding process. The compatibility was studied using test devices. MOS transistors which have polysilicon gate connected to the silicon substrate were not damaged, unless the heat treatment at the bonding temperature (400 °C) was so long as to make alloy spike at contact holes. Surface inversion under the field oxide was not occurred if the impurity concentration of the channel stopper is relatively high. Leakage current of pn junction was kept low enough especially by shielding its surface.

3.2.3
High vacuum sealing

High vacuum inside a cavity is required for capacitive vacuum pressure sensors, for resonators to reduce their dumping [10. Yoshimi et al. (1992)], and for thermal radiation sensors to reduce the heat dissipation [11. Cabuz et al. (1993)]. Pressure control inside a cavity is required for optimum dumping of the seismic mass in capacitive accelerometers [9. Mineta et al. (1993)]. In addition to these examples mentioned in the former paragraph, there are other purposes as vacuum microelectronic devices.

Since hot plate heating is not adequate for bonding in vacuum because of its poor heat transfer in vacuum, a vacuum furnace was used [14. Esashi et al. (1992)]. When a high voltage is applied in a reduced pressure ambient, voltage breakdown occurs based on the Paschen's law. It is not possible to apply the voltage required for bonding in certain vacuum range, and hence anodic bonding was difficult in the pressure range from 10^{-3} to 10 torr. However, the breakdown voltage was increased and consequently the pressure range of the bonding difficulty was made narrower (from 10^{-1} to 10 torr) by insulating the cathode lead wire with glass [17. Ura et al. (1992)].

Even if bonded in high vacuum, good vacuum could not be obtained in the cavity because oxygen gas was produced from the glass during the bonding process [17. Ura et al. (1992)]. To solve this problem, nonevaporable getter (NEG) was accommodated inside the cavity to adsorb the produced oxygen

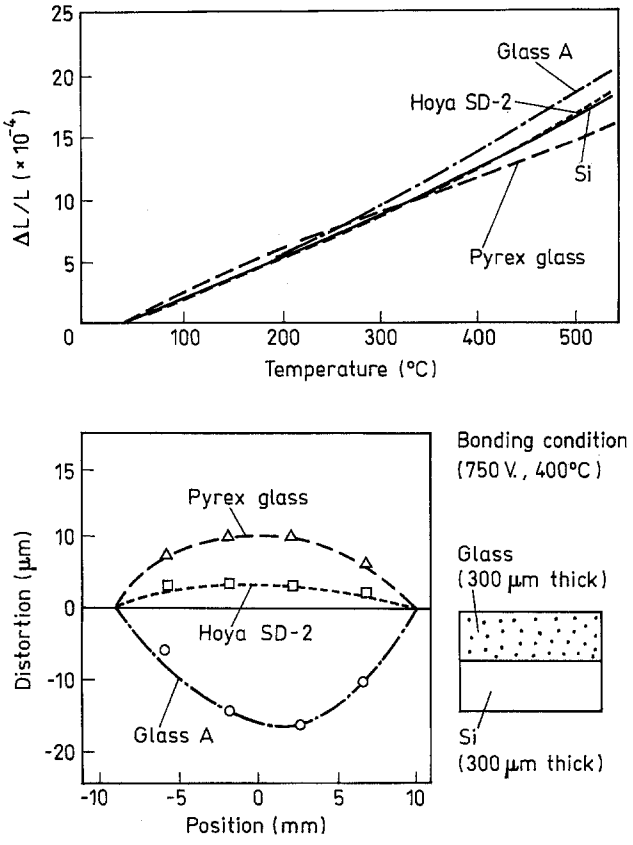

Fig. 10a, b. Thermal expansion properties and examples of distortion caused by anodic bonding. a Thermal expansion properties of glasses and silicon; b Examples of distortion after bonding

gas [4]. A capacitive vacuum pressure sensor using a piece of Zr–V–Fe getter is shown in Fig. 3. The activation of the getter material was carried out at 400 °C during the anodic bonding process. The pressure inside the cavity was lower than 1×10^{-5} torr and was not changed for more than 1 month.

3.2.4
Stress control

[18. Shoji et al. (1994)]

As the mismatch of thermal expansion coefficients of glass and silicon causes distortion after bonding, optimized bonding condition for minimum distortion was developed. Thermal expansion properties of some kinds of glass and silicon are shown in Fig. 10a. Examples of distrotion after anodic bonding using different kinds of glass are shown in Fig. 10b. The distortion observed can be explained qualitatively by the different thermal expansion of the glass in Fig. 10a.

Temperature drift of capacitive sensors are caused mainly by a packaging stress. At room temperature, silicon and Pyrex glass have different thermal expansion coefficients and the difference is assumed the major causes of the package related temperature drift. Recently glasses have been improved from this view point as shown in Fig. 10a.

Compositional change of the glass is caused by the alkaline ion migration during the bonding processes and this can induce the glass distortion. This effect was studied using a Pyrex glass which has aluminum films on both sides. Alkaline ion depletion

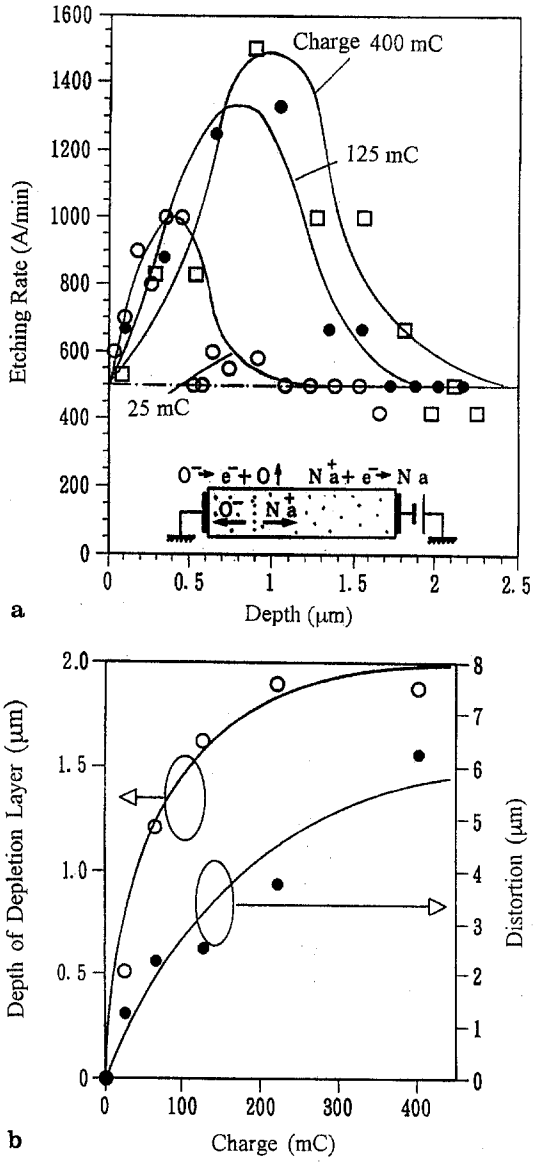

Fig. 11a, b. Glass distortion caused by alkaline ion depletion layer. a Depth profiles of glass etching rate; b Depletion layer thickness and distortion versus charge passed through the glass

layer is formed on the anodic side of the glass as shown in Fig. 11a. The depth of the depletion layer obtained from the glass etching rate and the distortion depend on the charge passed through the glass as shown in Fig. 11b.

3.3
Laser assisted etching

[19. Minami et al. (1993)]

Laser assisted silicon etcing has been developed and applied for three-axis accelerometer and resonators described above. Resistless dry etching is required to remove a part of silicon after anodic bonding. Figure 12a, shows the application of the laser assisted etching to an accelerometer. All parts of silicon including the feedthrough islands which is required for the structure shown in Fig. 9c should be connected with beams monolithically before anodic bonding. These beams have to be removed selectively after bonding. Fragile parts can be also

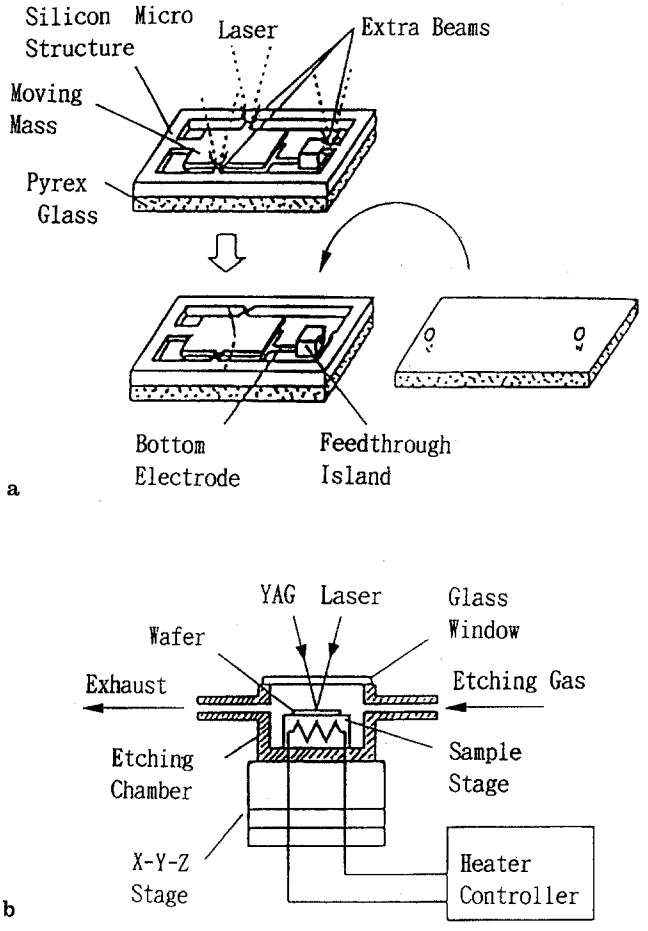

Fig. 12a, b. Laser assisted etching. a Application to accelerometer; b Apparatus

supported with extra beams as shown in Fig. 12a. This etching process allows the fabrication of the structure shown in Fig. 9c and has been used for three-axis accelerometer and resonant sensors described above.

YAG laser beam is focused on the silicon sample which is located in a etching chamber as shown in Fig. 12b. Reactive gases as HCl, SF_6 and NF_3 are used for the environment. This process makes fast and dry etching of silicon without particles feasible. The HCl gas has a drawback of damaging Al pattern. On the other hand, the SF_6 has a problem of redeposition of nonvolatile products. The NF_3 gas can solve these problems.

3.4
Advanced silicon etching

3.4.1
In-process thickness monitoring during silicon etching

[20. Minami et al. (1994)]

Diaphragm or beam structures are used in silicon micro-mechanical devices. The thickness of these structure strongly dominates their performances. In conventional wet etching, the thickness is controlled through etching time as well as p^+ or pn junction etch-stop technique. However, the etch-stop technique increase the complexity of the process and reduce the flexibility of the design.

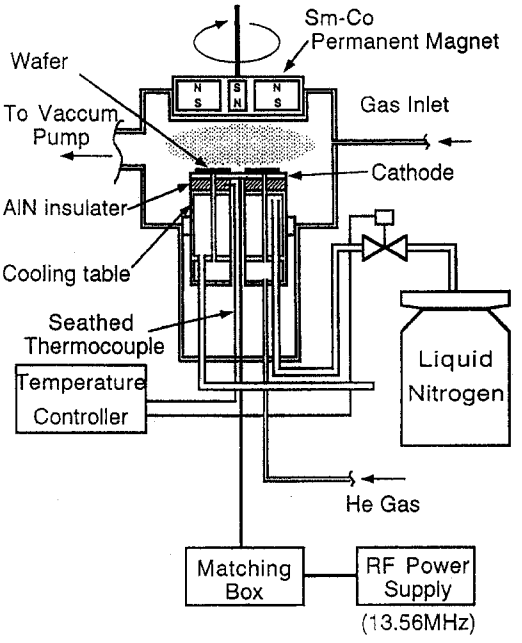

Fig. 13. RIE apparatus for deep silicon etching

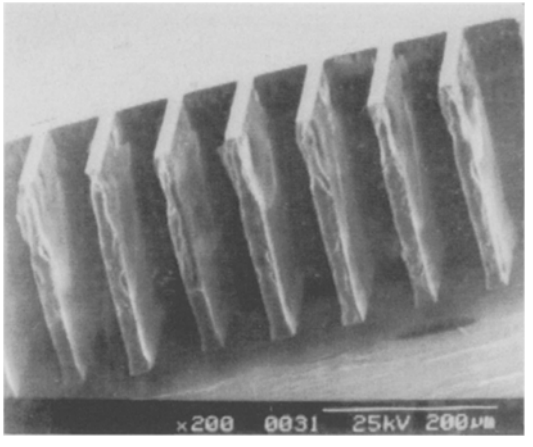

Fig. 14. Cross sectional view of etched through silicon wafer

A method for in-situ monitoring of the silicon thickness during anisotropic wet etching by TMAH (Tetramethyl Ammonium Hydroxide) was developed. The principle used is multiple-beam interference spectroscopy. Near infrared light ranging from 1000 nm to 1300 nm wave length was used and thickness from 2 μm to 20 μm could be measured. Transmission and reflection monitoring systems were developed.

3.4.2
Deep reactive ion etching of silicon

[21. Takinami et al. (1992)]

Reactive ion etching (RIE) was studied to fabricate silicon microstructures which have large aspect ratio. Deep and high rate directional dry silicon etching could be performed using the etching apparatus shown in Fig. 13. It has cooling table and permanent magnet. High flow rate of etching gas (SF_6) by using large vacuum pump and small etching chamber was effective to increase the etching rate. Etching rate of around 0.8 $\mu m\,min^{-1}$

with a small side etch ratio was achieved at −60 °C. Etching selectivity to the nickel mask was about 200. An example of the silicon wafer etched through 200 μm thickness is shown in Fig. 14. The RIE process has a limitation due to the dependency of the etching rate on the mask opening width, which is called micro loading effect.

4 Conclusion

Packaged micro sensors were fabricated using silicon micromachining. Glass-silicon anodic bonding which enables electrical feedthrough structures and two parallel plates which can be used for capacitive sensors and electrostatic actuators play an important role. Special micromachining technologies as laser assisted silicon etching and anodic bonding which enables to incorporate a circuit inside the package and to keep a sealed cavity at a high vacuum are developed. Integrated sensors as capacitive pressure sensors, accelerometers and resonating sensors have been realized as the packaged sensors. The feed-through structures have been also applied for other devices as piezoresistive pressure sensor [2. Esashi et al. (1990)], tactile imager [2. Esashi et al. (1990)], thermal mass-flow sensor [22. Esashi (1991)], two-dimensional optical scanner [23. Asada et al. (1994)] and linear electrostatic microactuator [24. Matsubara et al. (1993)].

Advanced intelligence as the communication interface for two-wires sensing system will be integrated [25. Esashi et al. (1991)] [7. Shirai et al. (1992)]. New technologies for example dry process machining of glass are expected.

References

1. **Esashi, M.:** (1990) Sensor Packaging; In: Reichl. H. "ed." (Micro System Technologies 90), pp. 495–502, Springer-Verlag, Berlin
2. **Esashi, M.; Matsumoto, Y.; Shoji, S.:** (1990) Absolute pressure sensors by air-tight electrical feedthrough structure, Sensors and Actuators, A21–A23: 1048–1052
3. **Matsumoto, Y.; Shoji, S.; Esashi, M.:** (1990) A miniature integrated capacitive pressure sensor, Tech. Digest of the 9th Sensor Sympt., 43–46
4. **Henmi, H.; Yoshimi, K.; Shoji, S.; Esashi, M.:** (1993) Vacuum packaging for micro sensors by glass-silicon anodic bonding, Transducers'93, 584–587
5. **Esashi, M.:** (1994) Sensor for measuring acceleration; In: de Rooij, N. "eds." (Mechanical Sensors (Sensors Vol. 7)), pp. 331–358, VCH Pub., Weinheim
6. **Matsumoto, Y.; Esashi, M.:** (1993) Integrated silicon capacitive accelerometer with PLL servo technique, Sensors and Actuators, A39, 209–217
7. **Shirai, T.; Ura, N.; Esashi, M.:** (1992) Two-wire silicon capacitive accelerometer, Trans of The IEICE Japan, J75-C-II, 554–562
8. **Jono, K.; Hashimoto, M.; Esashi, M.:** (1994) Electrostatic servo system for multi-axis accelerometers, Proc. IEEE MEMS'94, 251–256
9. **Mineta, T.; Yoshida, M.; Nomura, T.; Esashi, M.:** (1993) Capacitive accelerometers without fracture risk during fabrication processes, Transducers'93, 814–817
10. **Yoshimi, K.; Minami, K.; Wakabayashi, Y.; Esashi, M.:** (1992) Packaging of resonant sensors, Tech. Digest of the 11th Sensor Sympo., 35–38
11. **Cabuz, C.; Shoji, S.; Cabuz, E.; Minami, K.; Esashi, M.:** (1993) Highly sensitive resonant infrared sensor, Transducers'93, 694–697
12. **Cabuz, C.; Fukatsu, K.; Hashimoto, H.; Shoji, S.; Kurabayashi, T.; Minami, K.; Esashi, M.:** (1994) Fine frequency tuning in resonant sensors, Proc. IEEE MEMS'94, 245–250
13. **Hashimoto, M.; Cabuz, C.; Minami, K.; Esashi, M.:** (1994) Silicon resonant angular rate sensor using electromagnetic exitation and capacitive detection, Tech. Digest of the 12th Sensor Sympo., 163–166
14. **Esashi, M.; Ura, N.; Matsumoto, Y.:** (1992) Anodic bonding for integrated capacitive sensors, Proc. of IEEE MEMS'92, 43–48
15. **Shoji, S.; Esasi, M.:** (1990) Photoetching and electrochemical discharge drilling of Pyrex glass, Tech. Digest of the 9th Sensor Sympo., 27–30
16. **Shirai, T.; Esashi, M.:** (1992) Circuit damage by anodic bonding, JIEE Technical Meeting, ST-92-7, 9–17
17. **Ura, N.; Nakaichi, K.; Minami, K.; Esashi, M.:** (1992) Vacuum sealing by anodic bonding, The 11th Sensor Sympo., Late News, L1-1, 63
18. **Shoji, Y.; Suzuki, K.; Shoji, S.; Esashi, M.:** (1994) Reduced distortion anodic bonding, Micromachining Technical Report, The Japan Soc. of Next Generation Sensor Technology, MP-93-43, 53–66
19. **Minami, K.; Wakabayashi, Y.; Matsubara, T.; Yoshimi, K.; Yoshida, M.; Esashi, M.:** (1993) YAG laser assisted etching for releasing silicon micro structure", Proc. IEEE MEMS'93, 53–58
20. **Minami, K.; Tosaka, Y.; Esashi, M.:** (1994) Optical in-situ monitoring of silicon diaphragm thickness during wet etching, Proc. IEEE MEMS'94, 217–222
21. **Takinami, M.; Minami, K.; Esashi, M.:** (1992) High-speed directional low-temperature dry etching for bulk silicon micromachining, Tech. Digest of the 11th Sensor Sympo., 15–18
22. **Esashi, M.:** (1991) Micro flow sensor and integrated magnetic oxygen sensor using it, Transducers'91, 34–37
23. **Asada, N.; Matsuki, H.; Esashi, M.:** (1994) Silicon micromachined two-dimensional galvano optical scanner, The 6th Joint MMM-Intermag Conf., AR-17
24. **Matsubara, T.; Yamaguchi, M.; Minami, K.; Esashi, M.:** (1993) Stepping electrostatic microactuator, Transducers'93, 50–53
25. **Esashi, M.; Matsumoto, Y.:** (1991) Common two lead wires sensing system, Transducers'91, 330–333